42

Photopolymer-based Waveguide Holograms for Optoelectronic Interconnects Applications

Ray T. Chen, Charles Zhou, Chun-he Zhao and Richard Lee
Microelectronics Research Center
J. J. Pickle Research Campus
University of Texas, Austin
Austin, TX 78758
Email: raychen@uts.cc.utexas.edu

Abstract

In this paper, we report the implementation of waveguide-based holograms for several on-going applied photonics research at the Microelectronics Research Center of the University of Texas, Austin. These include a wavelength division demultiplexer (WDDM), a non-blocking wavelength-selective crossbar, an IEEE protocol compatible optical backplane bus and true-time-delay lines for wide-band phased array antennae. The exclusive characteristics of waveguide holograms and maturity of photopolymeric materials make the reported research findings highly attractive for system integration where device performance features and system reliability are pivotal.

The surface-normal configuration of both the WDDM and the wavelength-selective crossbar provides not only a much more rugged packaging due to the elimination of edge coupling but also an insertion compatibility with vertical cavity surface emitting laser integration. An eight channel wavelength division demultiplexing device with a center wavelength of 772 nm and a wavelength separation of 4 nm is demonstrated with channel to channel cross talk of less than -20 dB is experimentally confirmed in Section 2. A 3x3 crossbar with $\Delta\lambda$=10nm with a center wavelength of 765 nm is delineated in Section 3. An optical backplane bus containing nine memory/process boards with 72 interconnects is reported in section 4. A waveguide hologram based true-time-delay-line is presented in Section 5.

1. Introduction

Waveguide-based holographic optical elements (HOEs) are pivotal devices to provide several critical beam routing features that are not achievable through other means. Both micro- and macro-scale applications have been realized recently based on waveguide-based HOEs. Advancement in photopolymeric material has made the fabrication of both transmission and reflection holograms reliable and cost-effective over the wavelength span from UV to near IR. Among a myriad of feasible applications, optoelectronic interconnects is widely agreed to be one of the most plausible scenario where waveguide-based HOEs will play a key role

We recently built a surface-normal wavelength division multiplexer using photopolymer-based volume holograms in conjugation with graded index (GRIN) rod lenses[1]. The device configuration and the system demonstration are shown in Figure 2 where the multiple wavelength beams are provided through a Ti-Sapphire laser which can be replaced by a laser diode array with appropriate wavelengths. The elimination of edge-coupling significantly enhances the packaging reliability. Figure 2 shows the scheme for wavelength division demultiplexing (WDDM) we have demonstrated and the time reversal of the beam propagation automatically results in the required wavelength division multiplexing (WDM). Such a configuration is compatible with the implementation of vertical cavity surface-emitting lasers where surface-normal coupling is required. The waveguiding plate we employed supports substrate guided waves which are defined as substrate modes in conventional integrated optics terminology. The characteristic of azimuthal symmetry of the substrate modes is maintained in the waveguiding substrate when a TEM_{00} laser beam is employed as the signal carrier. Such a mode profile compatibility is expected to significantly reduce the coupling losses when compared with the conventional edge coupling between a waveguide and an optical fiber.

The experimental setup for an eight WDM shown in Fig.2 contains two independently recorded photopolymer-based waveguide holograms. The GRIN-lens-collimated light from the single mode fiber was diffracted by the input hologram and then zig-zagged within the waveguiding plate. Different wavelengths were diffracted with different bouncing angles. The intrinsic wavelength dispersion associated with the waveguide hologram provides us with an easy way to demultiplex optical signals solely based on wavelengths. The optical beams were subsequently coupled out by the output hologram. The output multi-wavelength beam pattern shown in the inset of Fig.2 is with a center channel wavelength of 772 nm (λ_4) and a wavelength separation of 4 nm. The output GRIN rod lens focused the light beams with different substrate bouncing angles to different spots representing different wavelengths. Such parameters as spot size, channel separation and crosstalk were measured.

In our experiment, the average channel separation was 80 μm and average spot size less than 60 μm which can be theoretically reduced to less than 5 μm. The average crosstalk was less than -20 dB. Current spot size is well-above the theoretical prediction due to the implementation of the 1/4-pitch GRIN lenses and the nature of Gaussian beam propagation within such GRIN lenses. The theoretical calculation shows that a 0.29-pitch GRIN lens will provide us with a diffraction-limited spot size. Note that the demonstrated device is operational bidirectionally. The time reversal of the presented scheme automatically provide us with the wavelength division multiplexing (WDM) where multiple wavelengths can be spatially multiplexed into one fiber.

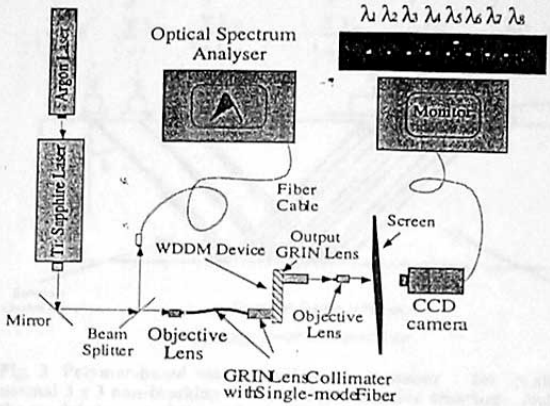

Fig. 2 Experimental setup for measuring the WDDM channel separation.

HOEs-based Optical Backplane

3. Surface-normal Wavelength Selective Cross Bar

Crossbar-based optical interconnects represents the most desirable network due to its fast switching speed and low latency in transmitting high speed signals. We report here the formation of a surface-normal non-blocking crossbar based on a unique wavelength switching scheme in which photopolymer-based volume holograms are employed in conjugation with graded index (GRIN) rod lenses. A prototype polymer-based volume hologram for multiple-wavelength 3 x 3 crossbar is experimentally demonstrated at 755, 765 and 775 nm. The unique beam routing property of a GRIN lens reduces nine wavelengths to three wavelengths while maintaining the required nine (3 x 3) individual interconnects. The elimination of edge-coupling significantly enhances the packaging reliability. Furthermore, such a configuration is compatible with the implementation of vertical cavity surface-emitting lasers where the characteristic of azimuthal symmetry may be maintained in the waveguide substrate [2].

The demonstrated device is shown in Fig. 3. The volume phase gratings recorded in the photopolymer films are slanted. The central wavelength of the input surface-normal beam, i.e., 765 nm, is designed to be diffracted with a maximum efficiency at the Bragg angle [3] which

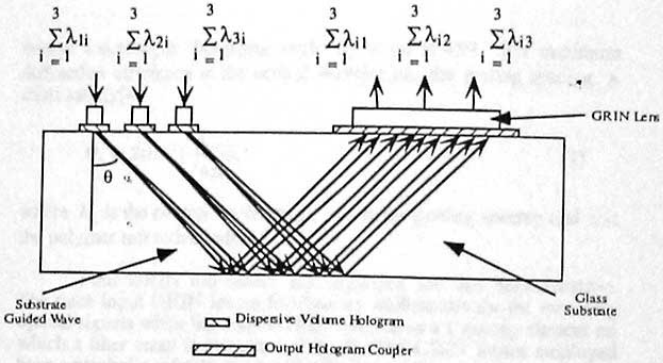

Fig. 3 Polymer-based volume hologram crossbar for a surface-normal 3 x 3 non-blocking wavelength selective crossbar. Note that the special characteristic of the GRIN lens reduces the nine wavelengths to three, i.e. $\sum_{i=1}^{3}\lambda_{i1} = \lambda_1 = 755\text{nm}$, $\sum_{i=1}^{3}\lambda_{i2} = \lambda_2 = 765\text{nm}$, **and** $\sum_{i=1}^{3}\lambda_{i3} = \lambda_3 = 775\text{nm}$.

is 45° in our design. The wavelengths that deviate from the center wavelength are dispersed at different substrate bouncing angles with less diffraction efficiencies where discrete substrate modes are generated and zig-zagged within the substrate[4]. The schematic of the micro-structure of the designed volume holograms is shown in Fig. 4. The

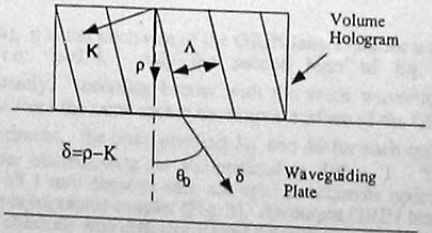

Fig. 4 Phase grating diagram showing phase-matching condition. K, ρ and δ represent the grating vector, the input wave vector and the output wave vector respectively.

central wavelength bouncing angle θ_0 is set at 45°. For maximum diffraction efficiency at the central wavelength, the grating spacing Λ must satisfy[4]:

$$\theta_0 = 2\sin^{-1}(\frac{\lambda_o}{2n\Lambda}), \quad (1)$$

where λ_o is the central wavelength, Λ is the grating spacing and n is the polymer refractive index.

Four GRIN rod lenses are employed for this demonstration. The three input GRIN lenses function as collimators for the incoming optical signals while the output GRIN rod lens as a focusing element on which a fiber array is integrated (Fig. 3). The GRIN lenses employed have a parabolic refractive index distribution profile of

$$n(y) = n(0)(1 - \frac{A^2}{2}y^2), \quad (2)$$

where n(0) is the refractive index of the GRIN lens axis and A is the GRIN lens property constant. The paraxial equation describing the ray position at the output GRIN lens surface from a zigzag substrate mode with a bouncing angle $\Delta\theta$ away from the Bragg condition is[5]:

$$y(L) = y_0 \cos(AL) + \frac{\tan(\Delta\theta)}{A} \cdot \sin(AL), \quad (3)$$

where

$$L = \frac{2\pi p}{A}. \quad (4)$$

In Eq. (4), p is the pitch size of the GRIN lens. Note for a quarter pitch lens, i.e., p=1/4, only the second term of Eq. (3) exists. Consequently, incoming beams with the same wavelength and $\Delta\theta$ come out from the same spot at the output surface of the GRIN lens. In our experiment, the corresponding λ_{ij} and $\Delta\theta$ for each case of the 3 x 3 crossbar interconnects are summarized in Table. 1. Three GRIN lenses with 1 mm diameter each are used to collimate optical signals to the input holographic coupler (Fig. 3). An output GRIN lens is used to separate channels with different zigzag bouncing angles. At the surface of output GRIN lens, rays with the same initial bouncing angle converge to the same spot as predicted by Eq. (3). Therefore, employment of GRIN lens reduces nine wavelengths to three wavelengths while keeping the required 3 x 3 interconnects. Combining

our crossbar with the fast switching wavelength tunable VCSEL[6], a non-blocking 3x3 crossbar interconnects with a nano-second (10^{-9}) switching speed can be realized. The bouncing angle differences are provided by the intrinsic dispersion of the input volume hologram. The use of GRIN lenses provides the capability of surface normal coupling through holograms and fibers. The vulnerable edge coupling scheme is eliminated. A reliable miniaturized packaging can thus be provided.

Table 1 Corresponding wavelengths and $\Delta\theta$s of the nine interconnects for 3 x 3 non-blocking crossbar.

Output \ Input	1	2	3
1	$\Delta\theta$=0.5° λ_{11}=755nm	$\Delta\theta$=0.5° λ_{21}=755nm	$\Delta\theta$=0.5° λ_{31}=755nm
2	$\Delta\theta$=0° λ_{12}=765nm	$\Delta\theta$=0° λ_{22}=765nm	$\Delta\theta$=0° λ_{32}=765nm
3	$\Delta\theta$=-0.5° λ_{13}=775nm	$\Delta\theta$=-0.5° λ_{23}=775nm	$\Delta\theta$=-0.5° λ_{33}=775nm

In the configuration shown in Fig. 3, three input fibers each with a collimating GRIN lens at its end are attached surface normally to the input volume hologram coupler. The three wavelengths transmitted through one single fiber are dispersed by volume hologram into hree different bouncing angles. The bouncing angle deviation from the center wavelength is described by the coupled wave theory [3] which gives

$$\Delta\theta = \frac{\Delta\lambda}{\lambda_0}\tan\theta_0, \qquad (5)$$

where λ_0 is the center wavelength, $\Delta\lambda$ is the wavelength deviation from the center wavelength and θ_0 is the bouncing angle for the center wavelength corresponding to the perfect phase matching condition. As described by Eq. (3), a quarter pitch output GRIN lens separates light beams with different bouncing angles. $\Delta\theta$ is experimentally determined to be $\pm 0.5°$ with $\lambda_0 = 765$ nm and $\theta_0 = 45°$. This results is in good agreement with the theory. The signal beams with a same wavelength from three separate input fibers are thus routed to the same spot at the output surface of the quarter pitch GRIN lens (Fig. 5), where a fiber array is attached (3 fibers in our case). Therefore by using only three wavelengths, a non-blocking 3 x 3 crossbar can be realized. The

address of the sender in this case can be identified through the header encoded in the optical signal [7].

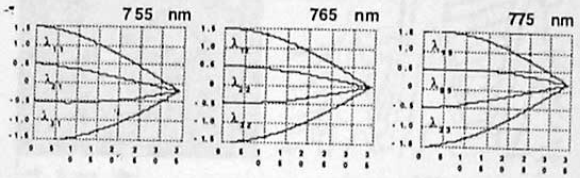

Fig. 5 Ray tracing of light with different incident angles from three input angular dispersed light beams onto the quarter pitch output GRIN lens (a) $\sum_{i=1}^{3}\lambda_{i1}=\lambda_1=755\text{nm}$, (b) $\sum_{i=1}^{3}\lambda_{i2}=\lambda_2=765\text{nm}$, (c) $\sum_{i=1}^{3}\lambda_{i3}=\lambda_3=775\text{nm}$.

The experiment is conducted using a p-polarized Ti:sapphire tunable laser pumped by a continuous Argon Ion laser. DuPont polymer film HRF-600 having a thickness of 20 μm is employed and the hologram is recorded at 514 nm. The volume hologram is fabricated using two beam interference method[8]. The central wavelength diffraction efficiency of 83% is experimentally obtained. A microscopic objective couples the light into a single mode fiber which has a GRIN rod lens attached at the output end. The input wavelength is monitored by an optical spectrum analyzer. The collimated light from the single-mode fiber is diffracted by the input holographic coupler and zig-zagged inside the glass substrate. It is subsequently coupled out by the output holographic coupler. The output GRIN rod lens focuses the light onto different spots corresponding to different wavelength channels. A CCD camera and an eight bit frame grabber image processing system is employed to take the pictures. Spot size, channel separation and other parameters are experimentally confirmed in Fig. 6. In our experiment, the average channel separation is 250 μm and average spot size less than 75 μm. The average crosstalk is less than -20 dB. The result is summarized in Table 2. 3 x 3 interconnects are experimentally confirmed. The result shown in Fig. 6 represents incoming optical signal from one input fiber having three different wavelengths. The output spectrum of 775 nm channel corresponding to the right spot shown in Fig. 6 is further illustrated in Fig. 7. The output spectrum has the same bandwidth as that of the input (not shown). It's also true for other channels. We have not observed any unwanted spectral shift due to scattering in all nine interconnects. The measured two-way insertion loss is less than 3 dB.

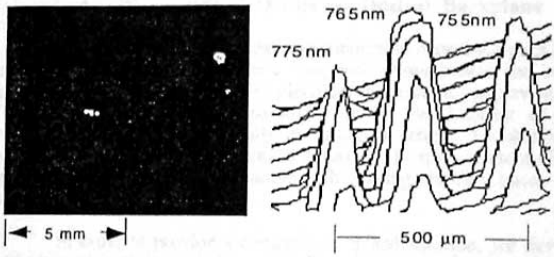

Fig. 6 (a) Image of GRIN lens output surface showing three-wavelength channel separation (b) Three-dimensional intensity profile of the three spots shown in Fig. 3(a).

Table 2 The measurement result of three-wavelength non-blocking crossbar.

Wavelength	Spot Size (3 dB)	Channel Separation
λ_1 = 755 nm	75 μm	250 μm
λ_2 = 765 nm	75 μm	
λ_3 = 775 nm	75 μm	

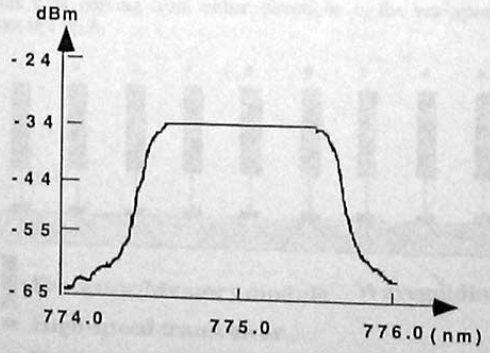

Fig. 7 One Output spectrum of the 3x3 crossbar (775 nm).

4. Waveguide-HOEs-based Optical Backplane

In an effort to increase the interconnection capacity, optics has been considered as an alternative for a long time. Nonetheless, the burden of electrical-to-optical and optical-to-electrical conversions has prevented optics from growing as a viable solution. Recent development of efficient optoelectronic devices, especially in forms of arrays, has stimulated the research seeking for feasible optical solutions. In spite of these efforts, no general optical backplane compatible with existing electrical buses has been announced.

In order to provide a competitive optical solution, we developed a bidirectional optical backplane. Unlike the previous optical backplanes aimed at special purpose computers, the backplane reported herein is for general purpose. It is compatible with standard multiprocessor backplane buses such as Futurebus+, Multibus II, etc.[2]. System demonstration containing nine processor/memory boards is described. Figure 8 shows the schematic of the bidirectional optical backplane in a multiprocessor system which has nine processor/memory boards. The backplane bus must provide a path for the bidirectional signal flow among the nine boards. To meet this goal, we employed an array of multiplexed holograms in conjunction with a waveguiding plate. Each electrical transceiver at the processor/memory board drives the corresponding laser diode located at the bottom of the board. The light from the laser is then bidirectionally coupled into the substrate through a multiplexed hologram. The surface-normal fanouts are provided by an array of holograms located between the backplane and the processor/memory boards. The photodiode associated with each signal line detects light coming from either directions in the waveguiding plate as shown in Fig. 8.

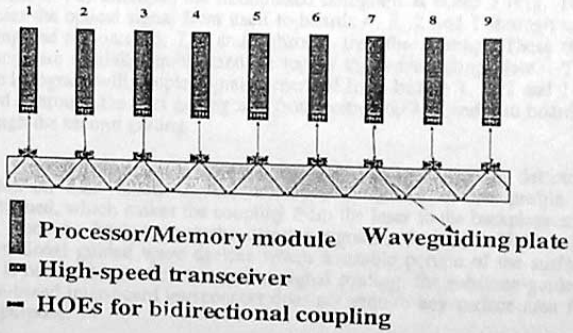

Fig. 8 Waveguide-HOE-based Optical Bidirectional Backplane Bus in a Multiprocessor System with nine Processor/Memory Boards.

The signal is coupled into the backplane through a hologram acting as an input coupler, which is designed to provide a total-internal-reflected (TIR) beam within the waveguiding plate. An array of multiplexed holograms are recorded along each signal path, as shown in Fig. 8.

A schematic illustrating the diffraction mechanisms associated with the multiplexed holograms is given in Fig. 9. In Fig. 9(a) $\vec{K}_1$ and $\vec{K}_2$ are the grating vectors corresponding to the two gratings recorded inside the polymer film. A surface-normal incident light with a wave vector $\vec{k}$ is phase-matched with both gratings, which have the same Bragg diffraction angle. As a result, two diffracted beams with wave vectors $\vec{k}_1'$ and $\vec{k}_2'$ are generated by the multiplexed hologram and converted into substrate-guided waves in two opposite directions as shown in Fig. 9(b). During the subsequent waveguiding processes, when the substrate-guided beam hits the multiplexed hologram with a Bragg angle, it gets diffracted generating optical signals necessary for the bidirectional optical backplane, as shown in Fig. 9(c). The light diffracted surface-normally out of the backplane has the wave vector $\vec{k}_{up}'$, and is detected by the photodiode, The light with the wave vector $\vec{k}'$ will provide power to the subsequent boards. The other surface-normal fanouts with the wave vector $\vec{k}_{down}'$ can be used for adding more boards on the opposite side of the waveguiding plate. The optimization of the diffraction efficiencies associated with each multiplexed hologram is needed to minimize the dynamic range of the power received at each board.

Each multiplexed hologram acts as an input coupler to split a surface normal TEM_{00} laser beam into two substrate-guided beams with a pre-designed bouncing angle of 45°. The same hologram couples a substrate-guided beam into a surface-normal fanout beam with a specific coupling efficiency. For example, the multiplexed hologram at board 5 (Fig. 10), couples the optical signal from itself to boards 4, 3, 2 and 1 through one grating and to boards 6, 7, 8 and 9 through the other grating. These two gratings are spatially multiplexed on top of the waveguiding plate. The same hologram will couple signals generated from boards 4, 3, 2 and 1 to board 5 through the first grating and from boards 6, 7, 8 and 9 to board 5 through the second grating.

The dots in Fig. 10 represent the input lights going to the detectors located on each board. Again, azimuthal symmetry of the profile is maintained, which makes the coupling from the laser to the backplane and then from the backplane to the detector significantly easy. Unlike the conventional guided wave devices where a sizable portion of the surface area is needed to provide the optical signal routing, the substrate-guided-wave-based inter-board interconnect does not require any surface area for this purpose.

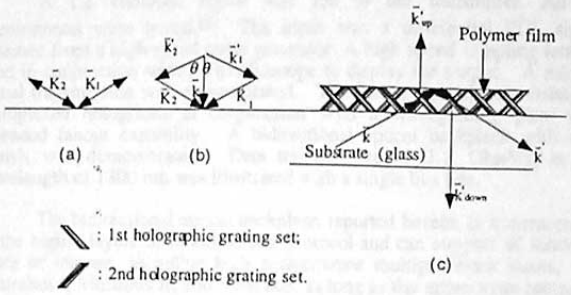

Fig. 9 Diffraction mechanism of light in by two sets of hologram gratings recorded on a glass substrate. (a). Two grating vectors recorded; (b). Light diffraction geometry by the gratings; (c). Light transmission, diffraction and reflection in side the bidirectional backplane bus.

The main advantage of our optical backplane stems from its ability to provide the cascaded fanouts with a signal flow in both directions. This concept is well illustrated in Fig. 10, which was taken from the surface-normal direction (Figure 8) and shows a set of photographs taken from the bidirectional backplane in the surface-normal direction. Each picture corresponds to a different case where one board is transmitting its signal to the other eight boards. The bidirectionality is demonstrated by the fact that the same multiplexed hologram can be used as both the input and the output couplers. The input beams are not shown in Fig. 10. The demonstration we provided contains 72 (8x9) interconnects for each backplane bus line.

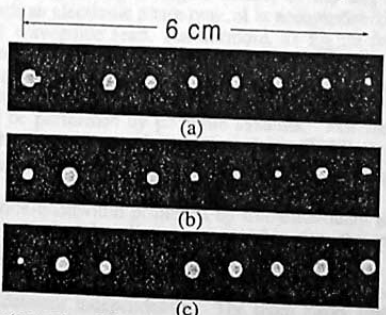

Fig. 10 Photographs with (a) the second, (b) the third, (c) the fourth boards sending optical signal to the other boards through the bidirectional optical backplane.

A 1.2 GBit/sec signal was fed to the transmitter. All 72 interconnects were tested.[9] The input was a differential ECL signal obtained from a high speed pulse generator. A high speed sampling head is used in conjunction with an oscilloscope to display the output. A reliable signal transmission was demonstrated. The optical backplane consists of multiplexed holograms in conjunction with a waveguiding plate with cascaded fanout capability. A bidirectional optical backplane with nine boards was demonstrated. Data transfer rate of 1.2 Gbit/sec at the wavelength of 1300 nm was illustrated with a single bus line.

The bidirectional optical backplane reported herein, is transparent to all the higher layers of electrical bus protocol and can support all kinds of buses of interest, including high performance multiprocessor buses, like Futurebus+, Multibus II, and VMEbus, as long as the appropriate protocols governing the rules of data transaction are provided. The result presented herein represents the first optical backplane fully compatible with IEEE standard backplane bus protocols.

5. Waveguide-HOEs-based True-Time Delay Lines for Phased Array Antennae

Phased-array antennae (PAA) offer many advantages, including steering without physical movement, accurate beam pointing, increased scan flexibility, precise elemental phase and amplitude control to obtain low spatial sidelobes, and reduced power consumption and weight. PAA systems combine the signals from as many as thousands of antenna elements to point a directive beam at some angle in space. The characteristics and angle of the beam are selected electronically across the array elements using analog or digital control of the amplitude and phase excitation. Such an electronic phase control is accomplished through bulky, heavy coaxial waveguide feed. Furthermore, as higher frequency phased array operation is pursued, element spacing will become increasingly tight, making waveguide congestion and crosstalk at the array backplane serious concerns. With the progress in photonic technology, most of these control functions can be performed by photonic systems. For instance, photonic systems can be used to provide true-time-delay (TTD) transmission paths for the microwave signals that are distributed to array elements.

The wide-bandwidth promised by true-time-delay is due to the fact that a fixed set of delay lines compensates for the path differences corresponding to a particular steering angle θ_o over an ultra large microwave bandwidth. Steering of the angle can be achieved by turning on and off each detector independently. The more delay lines we have, the more angular selections are provided. A schematic of HOE-based true-time-delay lines for phased array antennae applications is depicted in Figure 11.

The spatial multiplexibility and demultiplexibility of the reported demonstration generate more delay lines per area and therefore a more accurate angle selection system is provided. Although broad-band potential has long been recognized, the true-time-delay approach is not commonly implemented at present in electronics because it requires the use of heavy, bulky coaxial cable/waveguides serving as rf delay lines. Spatially multiplexed HOEs offers a light weight, compact solution to accomplish highly accurate true-time-delay steering of microwave phased array antennae. The bandwidth and delay time product of fiber-optic delay lines is limited only by the optical dispersion of the waveguiding plate. An optical delay line presented herein is eventually non-dispersive over the frequency range of interest due to the small tuning range of optical wavelength (1nm is equivalent to ~300GHz)[10]. For instance, for a 5-bit time shifter, the architecture shown in Fig. 6 shall consist of 32 (2^5) delay lines whose lengths are designed to be L_0, $L_0+\Delta L$, $L_0+2\Delta L$, $L_0+3\Delta L$, . . . and $L_0+31\Delta L$. The length can be represented by

$$L_1=L_0=2d\cdot\sec(\theta_1/2)$$
$$L_2=L_0+\Delta L=2d\cdot\sec(\theta_2/2)$$
$$\vdots$$
$$L_{31}=L_0+31\Delta L=2d\cdot\sec(\theta_{32}/2) \qquad (6)$$

After going through the guiding plate, the rf signals are delayed by the propagation times (t_0, $t_0+\Delta t$, $t_0+2\Delta t$, $t_0+3\Delta t$, $t_0+4\Delta t$,...., and $t_0+31\Delta t$) of its optical carrier in the 32 spatially multiplexed substrate guided waves. The detector array coupled to the waveguides serves as an optoelectronic switch that selects a designated delay time for radiating element it addresses. For example, by turning on the bias of the detector integrated on the waveguide surface (Fig. 11) with lengths of $L_0+2\Delta L$, $L_0+4\Delta L$, $L_0+6\Delta L$, we "turn off" the rf signal delayed by $t_0+2\Delta t$, $t_0+4\Delta t$, $t_0+6\Delta t$. A specific steering angle $\Delta\varphi$ can thus be selected based on the formula

$$\Delta\varphi/\Delta L = (2\pi fn)/c \qquad (7)$$

where n is the effective index of the waveguides, f is the microwave frequency and c is the speed of light. The proposed system will provide us with a better control of $\Delta\varphi$.

Optical fanout of various delay lines are accomplished by HOEs. These HOEs couple the light into and out of substrate modes from the surface-normal directions. By selecting the proper thickness for a

holographic film with a given index modulation, close to 100% diffraction efficiency has been realized for a desired reconstruction wavelength. Further increase in film thickness results in lower diffraction efficiency, a condition referred to as over-modulation. Diffraction efficiency can be controlled by varying the photo-exposure dosage or the ratio of the two interference beams.

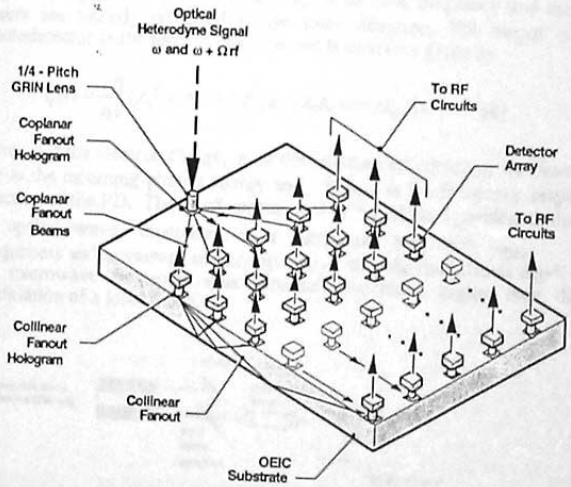

Fig. 11 HOEs-based Collinear and Coplanar True Time Delay Lines for Wide-band Phased Array Antennae Application

Uniform fan out intensity is required for a practical system. To ensure that the fanout optical signals from each output coupler are uniform in intensity, it is necessary to fine tune the diffraction efficiency from each output couplers shown in Fig. 11. With the coherent mixing of two CW lasers oscillating at single longitudinal frequencies, microwave frequency rf signals can be generated by the optical heterodyne technique. We employed two tunable diode lasers with a lasing wavelength around 786 nm. As indicated in Fig. 12, the outputs of the lasers are combined by a 50:50 beam splitter, passing an optical isolator and then coupled into the waveguide by a prism coupler at a suitable angle of incidence. Optical signal is coupled out of the waveguide through another prism coupler and then to a single mode fiber (SMF) with a 20 X microscope objective lens. The output of the

fiber is launched directly to an ultra fast photodetector through the matched FC connector. The current from photodetector (PD) is amplified through a broad band amplifier and immediately connected to a spectrum analyzer for display. The photocurrent output from the PD contains a DC part and an AC part corresponding to the high frequency rf beat signal. If the optical fields of two separate lasers are given by $E_1 = A_1 \exp(j\omega t)$ and $E_2 = A_2 \exp\{j(\omega + \omega_{12})t\}$, where ω_{12} is the beat frequency and the two lasers are linearly polarized in the same direction. The output of the photodetector in the form of photocurrent is therefore given by

$$i_c(t) = \frac{e\eta}{h\nu}(A_1^2 + A_2^2 + 2F(\omega_{12})A_1A_2\cos(\omega_{12}t)). \qquad (8)$$

Here, e is the electron charge, η is the quantum efficiency of the detector, $h\nu$ is the incoming photon energy and $F(\omega_{12})$ is the frequency response function of the PD. The result represented by Eq. (8) is equivalent to that of an optical wave, modulated at a microwave frequency ω_{beat}. The uniqueness and advantage of this approach is that the modulation depth and the microwave frequency thus generated are much higher than direct modulation of a laser diode.

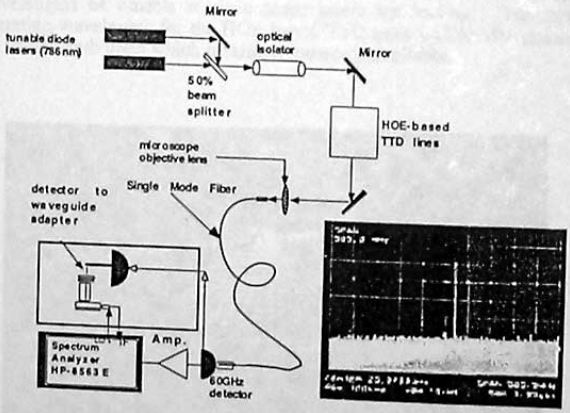

Fig. 12. Set-up of the generation of microwave signals by optical heterodyne detection.

With the set-up of Fig. 12, we have successfully produced and detected microwave frequency signals from 1 GHz up to the 25 GHz band. The inset of Fig.12 shows the detected 25 GHz rf signal by an spectrum analyzer. A signal to noise (S/N) ratio of ~ 20 dB is obtained. Presently, 25 GHz is limited only by the frequency response of the amplifier and the spectrum analyzer used. Realizing the fact that a small tuning of the laser wavelength (a few Å) will provide a large beat frequency, the task of generating wideband rf signals up to 100 GHz will be reported in the near future. In fact, microwave signals as high as several hundred gigahertz has already been achieved, only hindered by the difficulties of detecting and demonstration of such signals. By using external mixers and wideband amplifier, much higher upper frequency is expected. Feasibility of manipulating the HOE arrays shown in Fig. 11 with an accurate diffraction efficiency is further studied experimentally. One of the major challenges for the HOE-based TTD lines is the intensity of the heterodyne laser has to be strong enough to compensate the 1-to-n fanout loss. The maturity of external cavity semiconductor laser shall provide us with a reliable laser source. Figure 13 illustrates a massive fanout containing 30 delay lines using multiplexed holographic grating couplers developed. For the purpose of visibility, the operating wavelength of the device shown in Figure 8 is 514 nm. Each fanout beam is provided through the corresponding Bragg diffraction. The total diffraction efficiency is 92% with power fluctuation within ±3% among all 30 fanout beams. The holographic material we employed is highly transparent for both visible and near IR where all wavelengths of tunable semiconductor lasers are located. The optimal operating wavelength for the HOE-based TTD lines will be determined by the wavelength upon which maximum power is available.

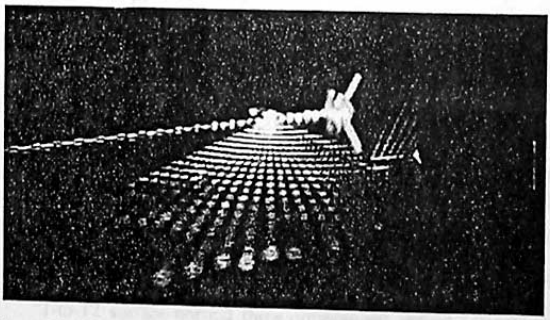

Figure 13 30 True-Time-Delay Lines Using a Multiplexed Waveguide HOEs containing 30 Holograms

6.0 Concluding Remarks

In this paper, we report the implementation of waveguide based HOEs for several on-going applied photonics research at the Microelectronics Research Center of the Univbersity of Texas, Austin. These include wavelength division multiplexer, non-blocking wavelength-selective crossbar, IEEE protocol compatible optical backplane bus and true-time-delay lines for wide band phased array antennae. The exclusive characteristics of waveguide holograms and maturity of photopolymeric materials make the reported research findings highly attractive for system integration where device innonativeness and system reliability are pivotal.

The reported research programs are currently sponsored by AFOSR, ONR, BMDO, ARPA's Center for Optoelectronics Science and Technology (COST), Cray Research, DuPont, Amoco, GE, Honeywell, Radiant Research and the State of Texas. We thank Drs. Charles Lee, Yoon-Soo Park and Bob Leheny for their support. Technical support from Dr. Willie Ng of Hughes Research Labs is also acknowledged.

7. References

1. "Five Channel Surface-normal Wavelength-division Demultiplexer using Substrate-guided Waves in conjunction with a Polymer-based Littrow Hologram", Optics Letters, Vol.20, 797-799(1995).
2. "Five-channel surface-normal wavelength-division demultiplexer using substrate-guided waves in conjunction with a polymer-based Littrow hologram ", Maggie M. Li and Ray T. Chen, Opt. Lett., Vol.20(7), pp.797, 1995.
3. "Coupled wave theory for thick hologram gratings", H. Kogelnik, The Bell Sys. Tech. J. 48(9), 2909 (1969).
4. "Two-channel surface-normal wavelength division demultiplexer using substrate guided waves in conjunction with multiplexed waveguide holograms ", Maggie M. Li and Ray T. Chen, Appl. Phys. Lett., Vol.66(3), pp.262-264, 1995.
5. "Matrix methods for the evaluation of lenses systems with radial gradient-index elements ", W. M. Rosenblum, J. W. Blaker and M. G. Block, American Journal of Optometry and Physiological Optics, Vol. 65, No. 8, pp. 661-665.
6. "Multiple wavelength tunable surface-emitting laser arrays", C. Chang, IEEE J. Quan. Electr. , Vol. 27, p. 1368 (1991).
7. IEEE Standard for Scalable Coherent Interface (SCI), IEEE STD 1596-1992.
8. "1-to-12 surface-normal three-dimensional optical interconnects ", R. T. Chen, S. Tang, M. M. Li, D. Gerold, and S. Natarajan, Appl. Phys. Lett. 63(14), 1883 (1993).

9. "Bi-directional Optical Backplane Bus for General Purpose Multi-Processor Board-to-Board Optoelectronic Interconnects," IEEE Journal of Lightwave Technology, Special Issue on Optical Interconnects, Vol. 13, pp. 1031-1040(1995).
10. "Holographic Optical Elements (HOEs) for True-Time-Delays Aimed at Phased Array Antenna Applications" Invited Paper to 1996 SPIE Photonics West, Vol.2689-25 (In Press).